The Mean Field Fokker–Planck Equation with Nonlinear No-flux Boundary Conditions

R. D. MILLS-WILLIAMS[*],

B. D. GODDARD[†],

G. A. PAVLIOTIS[‡]

March 29, 2022

Abstract

We consider the mean field Fokker–Planck equation subject to nonlinear no-flux boundary conditions, which necessarily arise when subjecting a system of Brownian particles interacting via a pair potential in a bounded domain. With the additional presence of an external potential V_1, we show, by analysing the linearised Fokker–Planck operator, that the spectral properties of the equilibrium densities can differ considerably when compared with previous studies, e.g., with periodic boundary conditions. Amongst other mean field models of complex many-body particle systems, we present numerical experiments encompassing in a wide range of physical applications, including: generalised exponential models (Gaussian, Morse); a Kuramoto model, for noisy coupled oscillators; and an Onsager model for liquid crystals. We showcase our results by using the numerical methods developed in the pseudospectral collocation scheme 2DChebClass.

1 Introduction

The theoretical study of systems of interacting particles is of vital importance for many physical, chemical and biological applications. Accurate models require the effects of many complex inter-particle interactions, such as, hard rods (Percus, 1976), spheres and disks (Rosenfeld, 1989; Roth, 2010; Roth et al., 2012), as well as mean field Coulombic interactions for electrostatic particles or charged particles in magnetic fields. Phase transitions are of central interest, in both experimental and computational studies, from, e.g., oxygen absorbed into tungsten (Gomer, 1990; Williams et al., 1978) to the freezing of hard and soft sphere fluids and crystal nucleation (Singh, 1991). For discrete models, kinetic phase transitions and chemical reactions in open systems have been modelled by use of lattice gas models (Zhdanov & Kasemo, 1994). In the social sciences, models of opinion dynamics demonstrate the existence of cluster formation in, for example, bounded confidence models of agents under the influence of characteristic leaders (Goddard et al., 2020; Hegselmann & Krause, 2015; Wang et al., 2017). More recently, phase transitions have been observed in continuum

[*]Institut für Theoretische Physik II: Weiche Materie, Heinrich–Heine–Universität Düsseldorf, Universitätsstraße 1, D–40225 Düsseldorf, Germany. Corresponding author: R. D. Mills-Williams (millswil@uni-duesseldorf.de).

[†]School of Mathematics and Maxwell Institute for Mathematical Sciences, University of Edinburgh, Edinburgh EH9 3FD, UK.

[‡]Department of Mathematics, Imperial College London, London SW7 2AZ, UK.

DDFT-SIR model of the transmission of the novel Covid-19 virus in a population (Te Vrugt et al., 2020).

In studying phase transitions, the choice of boundary conditions is important in determining admissible equilibrium states. In the aforementioned opinion dynamics models (Hegselmann & Krause, 2015; Wang et al., 2017), the choice of boundary conditions in the mean field description has been shown to be important in accurately predicting the onset of a phase transition, with the no-flux condition being the choice that most faithfully reproduces the underlying mechanisms in the associated deterministic models (Goddard et al., 2020). In classical inhomogeneous fluids, unbounded systems with a repulsive two-body inter-particle potential guarantee the existence of the uniform distribution as an equilibrium state (Martzel & Aslangul, 2001). Conversely, for purely attractive particles, clusters may form at sufficiently low temperatures due to the competition between diffusion and attraction (Dressler, 1987; Tamura, 1984). In periodic systems with even two-body potentials, the uniform distribution is a stable equilibrium solution, becoming unstable to perturbations at sufficiently small temperatures (Carrillo et al., 2019; Chayes & Panferov, 2010). For conserved mass systems in bounded domains, the no-flux condition precludes the uniform equilibrium state for many (but not all) even two-body potentials due to the asymmetric interaction between a particle at the boundary and in the bulk. In principle an external potential can be included to cancel out this effect, but the form of the potential is, for general systems, not expressible in analytical form.

Linear stability of equilibrium states in meanfield PDEs on the torus (i.e, with periodic boundary conditions) have been studied extensively. For simple two-body potentials, such as the Euclidean distance, the phase diagram for the noisy Hegselmann-Krausse model was first derived by Chazelle et al. (2017), delineating the parameter space for uniform, clustered, and coexisting equilibrium states. For extended applications, involving more exotic two-body potentials, (generalised Kuramoto (Kuramoto, 1981), Onsager model for liquid crystals (Chen et al., 2010), Barré–Degond–Zatorska model for interacting dynamical networks (Barré et al., 2017), Keller–Segel model for bacterial chemotaxis (Keller & Segel, 1971)) the full bifurcation diagrams were obtained by Carrillo et al. (2019).

Exact explicit expressions for non-uniform equilibrium states with vanishing flux at the boundary are given by Martzel & Aslangul (2001) for a few simple two-body potentials. However, they consider only a linear stability analysis around a uniform distribution arising for a limited number systems, and therefore forego an entirely general analysis. Additionally, therein, explicit equilibrium states were not found in the presence of a one-body potential, which is a restrictive for modelling. Furthermore, their linear stability analysis uses Fourier methods which assume periodicity, and hence cannot be applied to non-periodic equilibrium states. Alternatively, the linear stability of equilibrium states for the McKean-Vlasov equation with conserved mass on unbounded domains has been studied (Tamura, 1984) (in the presence of a confining potential), however only *sufficient* conditions for phase transition were possible to obtain, with strong assumptions on the set of permissible equilibrium densities and class of two-body potentials. In order to study the linear stability of general non-periodic densities, we here aim to develop non-Fourier methods for studying phase transitions in complex fluid systems subject to arbitrary one and two-body potentials.

1.1 Main Results.

The main contributions of the paper are threefold:

1. We present a linear stability analysis of the mean field Fokker–Planck Equation with nonlinear, nonlocal no-flux boundary conditions on a bounded domain.

2. We show the existence of bifurcations in non-periodic conserved mass systems, and recover a dispersion relation equivalent to the periodic case in the limit of weak interactions.

3. We use a sophisticated numerical method, based on a pseudospectral collocation scheme, to demonstrate the practical applications of the theoretical results.

1.2 Organisation of The Paper.

The paper is organised as follows: in Section 2 we present the governing equations of the time dependent density $\varrho(\mathbf{r},t)$ and equilibrium density $\varrho(\mathbf{r})$. In Section 3 we present a linear stability analysis of the mean field Fokker–Planck equation. In Section 4 we present some numerical experiments. Finally in Section 5 we discuss our results.

2 Equations of Motion

We consider $N \gg 1$ Brownian particles with unit mass and positions $\mathbf{r}^N = (\mathbf{r}_1, \cdots, \mathbf{r}_N)^\top \in \mathbb{R}^{d\times N}$, for $d \geq 1$, suspended in a background bath of many more, much smaller, and much lighter bath particles. It will be assumed that the dynamics of the bath particles relax to equilibrium on a faster timescale than that of the Brownian particles, and hence the intra-bath interactions may be treated via thermostated Langevin dynamics. In particular, the Brownian particles evolve according to the stochastic differential equations

$$\tfrac{\mathrm{d}\mathbf{r}_i}{\mathrm{d}t} = \nabla_{\mathbf{r}_i} V_1(\mathbf{r}_i) - \frac{\kappa_2}{N}\sum_{i\neq j}^{N} \nabla_{\mathbf{r}_i} V_2(|\mathbf{r}_i - \mathbf{r}_j|) + \sqrt{2\beta^{-1}}\boldsymbol{\zeta}_i(t) \tag{2.1}$$

where V_1 is a one-body potential, V_2 is a two-body potential with strength $\kappa_2 \in (0,\infty)$, $\beta \in (0,\infty)$ is the inverse temperature, and $\boldsymbol{\zeta}_t^i = \big(\zeta_i^1(t), \cdots, \zeta_i^d(t)\big)^\top$ is a d-dimensional Gaussian white noise process with $\langle \zeta_i^a(t)\rangle = 0$ and $\langle \zeta_i^a(t)\zeta_i^b(t')\rangle = 2\delta_{ij}\delta^{ab}\delta(t-t')$. The particles are assumed to be confined to a bounded physical domain, that is $\mathbf{r}_i(t) \in \Omega \subset \mathbb{R}^d$, $t \geq 0$, $i = 1, \cdots, N$. As such a constitutive boundary condition, e.g., an inelastic (momentum preserving) velocity condition must be imposed on $\partial\Omega$ in order to maintain $\mathbf{r}_i(t) \in \Omega$ for $t \in [0,\infty)$.

The corresponding PDE description of the particle trajectories evolving according to (2.1) is the Mean Field Fokker–Planck equation, given by

$$\partial_t \varrho = \nabla \cdot \left(\beta^{-1}\nabla\varrho + \varrho\nabla V_1 + \kappa_2\varrho\nabla V_2 \star \varrho\right), \tag{2.2}$$

which evolves the time dependent particle density $\varrho(\mathbf{r},t)$ at the position vector $\mathbf{r} \in \Omega$ and for time $t \in (0,\infty)$, where $\star$ denotes convolution in $\mathbf{r}$. The confinement of each particle to Ω in (2.1) necessarily implies the principle of conservation of mass in the mean field description (2.2), i.e., $\int_\Omega \mathrm{d}\mathbf{r}\, \varrho(\mathbf{r},t) = N$ where $N \in \mathbb{R}$ independent of time. As such (2.2) is subject to the nonlinear no-flux boundary condition

$$\mathbf{j}|_{\partial\Omega} \cdot \mathbf{n} = 0, \tag{2.3}$$

where $\mathbf{j} := -\left(\beta^{-1}\nabla\varrho + \varrho\nabla V_1 + \kappa_2\varrho\nabla V_2 \star \varrho\right)$ denotes the flux, and $\partial\Omega$ denotes the boundary of Ω.

The mean field Fokker–Planck equation (2.2), may be rigorously derived as the over-damped limit (neglecting inertial effects) of the Vlasov–Fokker–Planck equation, for which there exits a fully developed mathematical foundation on the existence and regularity of solutions, e.g., (Diperna & Lions, 1988; Victory Jr. & O'Dwyer, 1990). In the classical literature, one decouples V_2 from ϱ by writing $\tilde{V}_2 = V_2 \star \varrho$ and considering the auxiliary equation $\Delta\tilde{V}_2(\mathbf{r},t) = f(\varrho)$. In such a decoupling, $\tilde{V}_2$ may be viewed as the effective potential generated by the mass distribution $\varrho(\mathbf{r},t)$, and the function $f(\cdot)$ defines, e.g., a Poisson equation in the modelling of plasmas (Bouchut & Dolbeault, 1995; Hérau, 2007), or the Lame–Emden equation, in order to model the distributions of stars in a star clusters (Messer & Spohn,

1982). Here however, we preserve the nonlinearity in ϱ by maintaining the convolution term in (2.2).

One particularly interesting generalisation of (2.2) is Dynamic Density Functional Theory (DDFT) (Archer & Evans, 2004; Goddard et al., 2012a; Marconi & Tarazona, 1999), which expresses the mean field dynamics in gradient flow form by

$$\partial_t \varrho = \nabla \cdot \left(\varrho \nabla \tfrac{\delta \mathcal{F}}{\delta \varrho}[\varrho] \right), \tag{2.4}$$

for $\mathbf{r} \in \Omega$ and $t \in (0, \infty)$, where $\mathcal{F}[\varrho]$ is the Helmholtz free energy functional (which will be duly defined), and $\delta/\delta\varrho$ denotes functional differentiation, i.e.,

$$\frac{\delta \mathcal{F}}{\delta \varrho}[\varrho] := \lim_{\epsilon \to 0} \frac{\mathcal{F}[\varrho + \epsilon w] - \mathcal{F}[\varrho]}{\epsilon}$$

where w is a, suitably well behaved mean-zero function. The free energy functional $\mathcal{F}[\varrho]$ is given by

$$\mathcal{F}[\varrho] = \beta^{-1} \int \mathrm{d}\mathbf{r}\, \varrho \log \varrho + \int \mathrm{d}\mathbf{r}\, \varrho V_1 + \frac{\kappa_2}{2} \int \mathrm{d}\mathbf{r}\, \varrho V_2 \star . \varrho,$$

In the physics literature, $\mathcal{F}[\varrho]$ normally includes a de Broglie wavelength in the entropy term $\varrho \log \varrho$, denoting the average thermal volume of a particle in the bulk. We have set this constant to unity for simplicity.

The recasting of (2.2) into (2.4) is useful for analysing the convergence to equilibrium of time dependent densities in the sense of classical statistical mechanical measures, such as Kullback–Leibler divergence (equivalently relative entropy) but also for analysing the behaviour of the free energy of equilibrium densities parametrised by the interaction strength κ_2. In either form, (2.2) or (2.4), the equilibrium density $\varrho(\mathbf{r})$ satisfies

$$\nabla \cdot \left(\beta^{-1} \nabla \varrho + \varrho \nabla V_1 + \kappa_2 \varrho \nabla V_2 \star \varrho \right) = 0. \tag{2.5}$$

It can be equivalently shown that by a classical fixed point argument (e.g., see Dressler (1987), Theorem 1)) equilibrium density fields ϱ satisfying (2.5), together with the boundary condition (2.3), also satisfy the self consistency equation

$$\varrho = \frac{e^{-\beta(V_1 + \kappa_2 V_2 \star \varrho)}}{Z(\varrho)}, \tag{2.6}$$

where $Z(\varrho) = \int \mathrm{d}\mathbf{r}\, e^{-\beta(V_1 + \kappa_2 V_2 \star \varrho)}$, for fixed κ_2. In particular, for $V_1 \in C^\infty(\Omega)$ and $V_2 \in C_b^\infty(\Omega)$ then one has a smooth density ϱ satisfying (2.6), and for β inside a critical region defined by $\beta\kappa_2 \leq 1/4\|V_2\|_\infty^{-1}$, ϱ is unique.

Note that in (2.5) and (2.6), the equilibrium density is essentially parametrised κ_2 or β, one being redundant. Without loss of generality, as β varies outside the critical region qualitatively different density profiles will emerge (see, e.g., (Dressler, 1987, Sec. 4, Theorem 1)).

We prescribe (2.2) with suitably well behaved initial data $\varrho_0(\mathbf{r})$ given by equilibrium densities solving the self consistency equation (2.6). Additionally, we consider V_2 with sufficient decay on the boundary $\partial\Omega$ such that the integrals in (2.2), (2.3) converge, as well as having sufficient smoothness such that solutions ϱ are well behaved. We note that by varying the sign of V_2 we may explore the emergence of both clustered and non clustered densities.

3 Linear Stability Analysis

In this section we examine the stability properties of (2.2). As is standard in linear stability analyses, we seek to determine an expression for the eigenvalues of the corresponding linearised elliptic operator. We assume that $\beta\kappa_2 \leq 1/4\|V_2\|_\infty^{-1}$ (so that steady state is unique)

and linearise around the equilibrium density ϱ' by writing

$$\varrho = \varrho' + \epsilon\, w + O(\epsilon^2), \tag{3.1}$$

where $w = O(1)$ is a mean zero function and $\epsilon \ll 1$ is an arbitrary small parameter. Discarding all terms of order greater than unity, and dropping primes, one obtains

$$O(\epsilon^1): \qquad \partial_t w = \mathcal{L}_\varrho w := \beta^{-1}\Delta w + \nabla\cdot(w\nabla(V_1 + \kappa_2 V_2 \star \varrho)) + \kappa_2\nabla\cdot(\varrho\nabla(V_2\star w))\,. \tag{3.2}$$

We remark that the operator $\mathcal{L}_\varrho$ is different to the one found in previous linear stability analyses, e.g. (Carrillo et al., 2019, Sec 3.2), due to the inclusion of the background field and the fact that ϱ is generally non-uniform. Additionally, in order to conserve mass, perturbations must be mean zero for all time t, that is $\int \mathrm{d}\mathbf{r}\, w = 0$, which may be seen by combining the conservation of mass with the perturbation expansion (3.1), one has

$$N = \int \mathrm{d}\mathbf{r}\, \varrho + \epsilon \int \mathrm{d}\mathbf{r}\, w + O(\epsilon^2),$$

where it will be recalled that N is the number of particles. The assumption that ρ is a number density (i.e., $\int \mathrm{d}\mathbf{r}\, \varrho = N$ for all time) will be useful later on, where N acts as a anti-stiffening parameter in our numerical experiments (see Section 4).

We linearise the nonlinear no-flux condition (2.3) to find the linearised boundary condition to accompany (3.2). In particular, we define the boundary operator $\Pi^{\kappa_2}[w]$ and find

$$O(\epsilon^1): \qquad \Pi^{\kappa_2}[w]\Big|_{\partial\Omega}\cdot\mathbf{n} := \varrho\nabla\left(\beta^{-1}\varrho^{-1}w + \kappa_2 V_2\star w\right)\Big|_{\partial\Omega}\cdot\mathbf{n} = 0. \tag{3.3}$$

For the linear operator $\mathcal{L}_\varrho$, we introduce the weighted Sobolev space $H^2(\Omega,\varrho^{-1})$ defined as

$$H^2(\Omega,\varrho^{-1}) := \left\{ u:\Omega\to\mathbb{R} \quad | \quad \sum_{|\alpha|<2} \|D^\alpha u\|^2_{L^2(\Omega,\,\varrho^{-1})} < \infty \right\},$$

where the weighted norm is given by

$$\|f\|^2_{L^2(\Omega,\,\varrho^{-1})} := \int \mathrm{d}\mathbf{r}\, \varrho^{-1}|f(\mathbf{r})|^2, \quad \text{for each } f\in L^2(\Omega).$$

Additionally, it may be shown that, (see, e.g., (Bertini et al., 2010, Proposition 2.6, Proposition 2.7)), $\mathcal{L}_\varrho$ is essentially self-adjoint, with a pure point spectrum and compact resolvent. Therefore from the classical theory of elliptic operators, $\mathcal{L}_\varrho$ possesses eigenfunctions forming a complete, orthonormal basis of $H^2(\Omega,\varrho^{-1})$, with a corresponding discrete spectrum of eigenvalues parametrised by κ_2, denoted $\{w_n(\mathbf{r};\kappa_2)\}_{n=0}^\infty$ and $\{\lambda_n(\kappa_2)\}_{n=0}^\infty$ respectively. The eigenfunctions $w_n(\mathbf{r};\kappa_2)$ and eigenvalues $\lambda_n(\kappa_2)$ satisfy

$$\mathcal{L}_\varrho w_n(\mathbf{r};\kappa_2) = \lambda_n(\kappa_2) w_n(\mathbf{r};\kappa_2), \tag{3.4a}$$

$$\Pi^{\kappa_2}[w]\Big|_{\partial\Omega}\cdot\mathbf{n} = 0. \tag{3.4b}$$

3.1 Eigenvalues for Weak Interactions

We note that the eigenvalue problem (3.4a) has no general solutions without considering particular choices of V_1 and V_2. Thus an expression for eigenvalues $\lambda_n(\kappa_2)$ can only be obtained on a case by case basis. In 1D, for a limited number of choices of V_2, one can obtain an expression for largest eigenvalue λ in a neighbourhood of the bifurcation point by perturbation methods (Chavanis, 2014; Chavanis et al., 2005).

We consider a similar analysis with a perturbative approach, by expanding the density field ϱ and the eigenfunctions $w(\mathbf{r};\kappa_2)$ in a power series of κ_2, such that $\beta\kappa_2 \ll 1$. In this regime two-body interactions are assumed to be weak, and temperature is order unity but above the critical temperature, so that ϱ is unique. In particular $\beta\kappa_2 < 1/4\|V_2\|_\infty^{-1}$. By using (2.6) we have

$$\begin{aligned}\varrho &= \frac{e^{-\beta V_1}}{\int \mathrm{d}\mathbf{r}\, e^{-\beta V_1}}\left(1-\beta\kappa_2\frac{\int \mathrm{d}\mathbf{r}\, e^{-\beta V_1}V_2\star\varrho}{\int \mathrm{d}\mathbf{r}\, e^{-\beta V_1}}+O(\kappa_2^2)\right)^{-1}\left(1-\beta\kappa_2 V_2\star\varrho+O(\kappa_2^2)\right)\\ &= \frac{e^{-\beta V_1}}{\int \mathrm{d}\mathbf{r}\, e^{-\beta V_1}}+\beta\kappa_2\left(\frac{\int \mathrm{d}\mathbf{r}\, e^{-V_1}V_2\star\varrho}{\int \mathrm{d}\mathbf{r}\, e^{-V_1}}-V_2\star\varrho\right)+O(\kappa_2^2).\end{aligned} \tag{3.5}$$

We note that the power series expansion (3.5), remains an implicit expression for the density field ϱ and is therefore not entirely useful. However, we see that, to leading order, ϱ can be approximated as the background density due to the one-body potential V_1.

For $w_n(\mathbf{r};\kappa_2)$ we use the ansatz

$$w_n(\mathbf{r};\kappa_2) = w_n^{(0)}(\mathbf{r})+\kappa_2 w_n^{(1)}(\mathbf{r})+\kappa_2^2 w_n^{(2)}(\mathbf{r})+\cdots. \tag{3.6}$$

Inserting both (3.5) and (3.6) into (3.4a) we obtain at leading order

$$O(\kappa_2^0): \qquad \beta^{-1}\Delta w_n^{(0)}+\nabla\cdot\left(w_n^{(0)}\nabla V_1\right)=\lambda w_n^{(0)}. \tag{3.7}$$

We must also perform a boundary condition transfer on (3.3). We obtain, at leading order,

$$O(\kappa_2^0): \qquad \phi_1\nabla\left(\beta^{-1}\phi_1^{-1}w\right)\Big|_{\partial\Omega}\cdot\mathbf{n}=0, \tag{3.8}$$

where $\phi_1 := \exp(-\beta V_1)/\int \mathrm{d}\mathbf{r}\,\exp(-\beta V_1)$. We note that (3.7), with the no-flux boundary condition (3.8) has no general analytical solution save for a limited number of choices of V_1. For example, in the case of the trivial background field $V_1\equiv 0$, the $w_n^{(0)}$ are eigenfunctions of the Laplacian. Alternatively, in 1D, for the case $V_1=\frac{1}{2}x^2$ the $w_n^{(0)}$ are Hermite polynomials.

At the next order we obtain

$$O(\kappa_2^1): \quad \beta^{-1}\Delta w_n^{(1)}+\nabla\cdot\left(w_n^{(1)}\nabla V_1\right)+\nabla\cdot\left(w_n^{(1)}\nabla V_2\star\phi_1\right)+\nabla\cdot\left(\phi_1\nabla V_2\star w_n^{(1)}\right)=\lambda w_n^{(1)}, \tag{3.9}$$

subject to the boundary condition

$$O(\kappa_2^1): \qquad \phi_1\nabla\left(\beta^{-1}\phi_1^{-1}w+V_2\star w\right)\Big|_{\partial\Omega}\cdot\mathbf{n}=0.$$

Similarly, (3.9) with boundary condition has no general analytical solution save for one restricted case which we now consider.

3.1.1 Zero Background Field on the Hypercube

In this section we consider Ω to be the d-dimensional cube in the case of zero background field, i.e., $V_1\equiv 0$. Thus we have that $\phi_1 = L^{-d}$, and (3.7) becomes

$$\beta^{-1}\Delta w_n^{(0)} = \lambda w_n^{(0)},$$

subject to

$$\nabla w_n^{(0)}\Big|_{\partial\Omega}\cdot\mathbf{n}=0,$$

and hence $w_n^{(0)}(\mathbf{r}) = M_n \prod_{i=1}^d w_{n_i}(r_i)$ where

$$w_{n_i}(r_i) = \begin{cases} \cos \frac{2\pi n_i}{L} r_i & n_i > 0, \\ 1 & n_i = 0, \end{cases}$$

and M_n is defined as

$$M_n = \frac{1}{L^{d/2}} \prod_{i=1}^d (2 - \delta_{n_i,0})^{1/2}.$$

Additionally (3.9) becomes

$$\beta^{-1} \Delta w_n^{(1)} + L^{-d} \nabla \cdot \left(\nabla V_2 \star w_n^{(1)} \right) = \lambda w_n^{(1)},$$

subject to

$$\nabla \left(\beta^{-1} L^d w_n^{(1)} + V_2 \star w_n^{(1)} \right) \Big|_{\partial\Omega} \cdot \mathbf{n} = 0, \tag{3.10}$$

where we have observed that $\nabla \cdot \left(w_n^{(1)} \nabla V_2 \star \phi_1 \right) = 0$ since $\phi_1 = L^{-d}$ is constant. In this case the eigenfunctions are given by

$$w_n^{(1)}(\mathbf{r}) = \left\{ L^{-\frac{d}{2}} e^{i \frac{2\pi}{L} n \cdot \mathbf{r}} \right\}_{n \in \mathbb{Z}^d \setminus \{\mathbf{0}\}}.$$

Additionally, the boundary condition (3.10) is trivially satisfied due to periodicity of the eigenfunctions. The eigenvalues λ_n are given by the expression

$$\lambda_n = \left(-\beta^{-1} \left(\frac{2\pi |n|^2}{L} \right)^2 - L^{-d} \left(\frac{2\pi |n|^2}{L} \right)^2 \hat{V}_2(n) \right)$$

which defines the critical temperature, β_c, in terms of the Fourier transform of the two-body kernel

$$\beta_c := -\frac{L^d}{\min_{n \in \mathbb{Z}^d \setminus \{\mathbf{0}\}} \hat{V}_2(n)}. \tag{3.11}$$

Equation (3.11) tells us that, for weak interactions, equilibria are unstable to perturbations if V_2 has a negative Fourier mode (c.f., periodic case Carrillo et al. (2018)).

3.2 Thermodynamical Stability

Density fields ρ that satisfy the self consistency equation (2.6) will be local minima of $\mathcal{F}$ if and only if $\delta^2 \mathcal{F} > 0$ for all perturbations w such that $\int \mathrm{d}\mathbf{r}\, w(\mathbf{r}) = 0$. We let $\epsilon \ll 1$ and observe the Taylor development of $\mathcal{F}$

$$\begin{aligned} &\mathcal{F}[\varrho + \epsilon w] - \mathcal{F}[\varrho] \\ &= \beta^{-1} \int \mathrm{d}\mathbf{r}\, (\varrho + \epsilon w) \left(\log \varrho + \tfrac{\epsilon w}{\varrho} - \tfrac{\epsilon^2 w^2}{2\varrho^2} + O(\epsilon^3) \right) + V_1(\varrho + \epsilon w) + \tfrac{\kappa_2}{2} (\varrho + \epsilon w) V_2 \star (\varrho + \epsilon w) - \mathcal{F}[\varrho] \\ &= \epsilon \int \mathrm{d}\mathbf{r}\, w(\mathbf{r}) \left(\beta^{-1} \log \varrho + \beta^{-1} + V_1 + \kappa_2 V_2 \star \varrho \right) + \frac{\epsilon^2}{2} \int \mathrm{d}\mathbf{r}\, \kappa_2 w(\mathbf{r}) V_2 \star w + \tfrac{\beta^{-1} w^2(\mathbf{r})}{\varrho} + O(\epsilon^3). \end{aligned}$$

Hence, by inspecting the coefficient of the order ϵ^2 term above, the second variation of $\mathcal{F}$ is given by,

$$\delta^2 \mathcal{F}[\varrho] = \tfrac{\kappa_2}{2} \int \mathrm{d}\mathbf{r}\, w(\mathbf{r}) V_2 \star w + \tfrac{\beta^{-1}}{2} \int \mathrm{d}\mathbf{r}\, \tfrac{w^2(\mathbf{r})}{\varrho}, \tag{3.12}$$

which we observe has no explicit dependence on V_1, but will have functional dependence through the density field ϱ. Recall that in general, due to the presence of V_1, density fields are spatially inhomogeneous. The expression (3.12) is useful in characterising the critical instability of an equilibrium density, since one only need find one mean zero function to break the positivity $\delta^2\mathcal{F}[\varrho]$.

To complement the analytical dispersion relation (3.11) and stability characterised by (3.12), for order unity two-body interactions we provide an existence result for bifurcations based on a weaker version of Crandall Rabinowitz theorem (Carrillo et al., 2019; Crandall & Rabinowitz, 1971). This is achieved by analysing the behaviour of the zeros of the nonlinear equation (2.6), instead of trying to solve the eigenvalue problem analytically. We find that the strength of the result achievable is restricted because above the critical temperature ϱ is not necessarily uniform, nor indeed not be an even function due to the presence of an external potential V_1. Since the calculations are routine we leave the details to Appendix B, and now consider numerical solutions to the full eigenvalue problem (3.4a)–(3.4b).

4 Numerical Experiments

In this section we present numerical experiments to demonstrate the physical applications of the linear stability theory, as developed in the previous sections, for a range of different two-body interaction kernels in conserved systems. We present numerical solutions of both the equilibria, given by (2.6), and dynamics, given by (2.4) for prescribed N, κ_2 and ξ, the number of particles, two-body interaction strength and characteristic interparticle attraction/repulsion length scale for V_2 respectively. For the equilibrium densities we solve the Euler-Lagrange equations given by

$$\begin{cases} \nabla \frac{\delta \mathcal{F}}{\delta \varrho}[\varrho](\mathbf{r}) = \mathbf{0}, \quad \text{for } \mathbf{r} \in \Omega = [-L,\, L], & \text{(4.1a)} \\ \int \mathrm{d}\mathbf{r}\, \varrho(\mathbf{r}) = N. & \text{(4.1b)} \end{cases}$$

where, in 1 dimension, L is the half length of an interval. We observe that numerical solutions of equations (4.1a)–(4.1b) are equivalent to numerical solutions of the self consistency equation (2.6), albeit the former requiring the determination of an integration constant (physically corresponding to the chemical potential). We choose to solve (4.1a)–(4.1b) over (2.6) to make the connection with the usual equations encountered in (D)DFT literature, (see, e.g., Goddard et al. (2016, 2012a,b); Nold et al. (2017)).

For the dynamic densities we solve (2.4), (2.3). For all the numerical computations, the nonlocal terms in (2.4), both in the evolution equation and the boundary condition, require efficient and accurate quadrature. We demonstrate the efficiency and accuracy of the pseudospectral collocation scheme 2DChebClass (Goddard et al., 2017), which is a freely available suite of numerical solvers for DDFT problems. In each of the presented numerical examples we used a minimum of 50 spectral collocation points. For a more detailed explanation of pseudospectral methods for DDFT problems, and for a detailed discussion on the efficient computation of convolution integrals, see (Nold et al., 2017).

Forgoing an in depth numerical analysis of the pseudospectral method applied to nonlinear Fokker–Planck equations, we note that in each example our numerical solutions are strictly positive on Ω. This is achieved by transforming the density field via the map $z = \exp\{\beta(V_1 - \varrho)\}$ and solving in exponential space for z before inverting back for ϱ. Strict positivity of our equilibria is not only physically realistic, but also consistent with the regularity dictated by Proposition 1 in Appendix A.

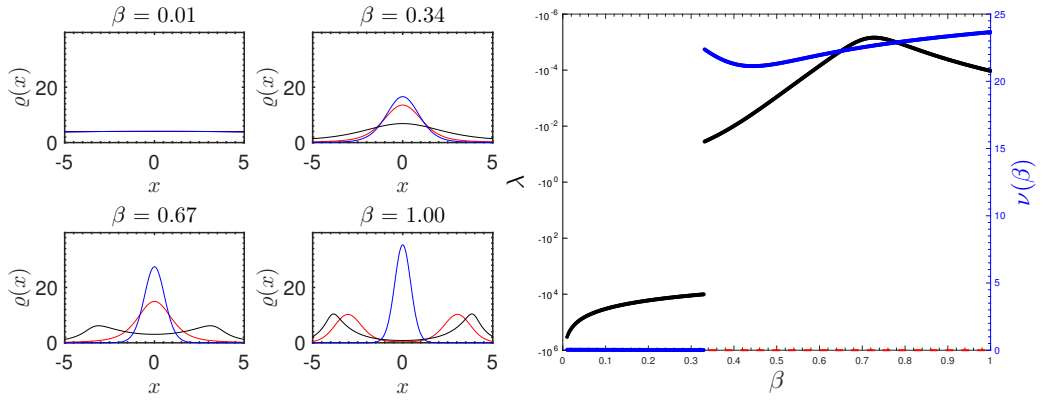

(a) (b)

Figure 1: Plots of (a) initial equilibrium densities $\varrho(\mathbf{r})$ (black solid), transient density $\varrho(\mathbf{r}, t)$ (red solid), perturbation function $u(\mathbf{r})$ (magenta solid), final equilibrium $\varrho(\mathbf{r}, t_*)$ (blue solid) for the Gaussian attractive kernel (4.3) $\{L,\, \kappa_2,\, \xi,\, N\} = \{5.0,\, 0.5,\, 1.9,\, 40\}$. (b) the minimum eigenvalue of (3.4a) (left, black solid) on a log scale, and the order parameter $\nu(\beta)$ with two solution branches: stable (right, blue solid) and unstable (red dashed).

4.0.1 Order Parameter

In order to characterise bifurcations we define the following order parameter, $\nu(\beta)$ as a function of the inverse temperature β, as (for a fixed interaction strength κ_2)

$$\nu(\beta) := \int \mathrm{d}\mathbf{r}\, w_1(\mathbf{r}; \kappa_2)\varrho(\mathbf{r}), \tag{4.2}$$

where $w_1(\mathbf{r}; \kappa_2)$ is the eigenfunction associated to the smallest eigenvalue $\lambda(\kappa_2)$ for each $\kappa_2 \in \mathbb{R}$ and $\varrho(\mathbf{r})$ is an equilibrium density. The order parameter $\nu(\beta)$ is analogous to the first Fourier mode of ϱ in the periodic setting (see, e.g., Carrillo et al. (2019)). The bifurcation diagrams are obtained as follows: for a given interaction strength κ_2, the equilibrium density ϱ is obtained by a pseudospectral collocation scheme applied to (4.1a)–(4.1b). To examine the stability of the bifurcated densities, we define a function $\varrho_p = \varrho + \epsilon u$ (where $\epsilon \ll 1$, u is mean zero, e.g., a sinusoid), as initial data for (2.4), (2.3). We let the transient density $\varrho(\mathbf{r}, t)$ relax to an equilibrium state $\varrho(\mathbf{r}, t_*)$, for sufficiently large t_*, such that $\varrho(\mathbf{r}, t_*)$ no longer varies in time. Stability was then characterised by whether or not $\varrho(\mathbf{r}, t_*) \equiv \varrho$. Then, $\nu(\beta)$ in (4.2) is computed using $\varrho(\mathbf{r}) = \varrho(\mathbf{r}, t_*)$. Additionally we compute $\lambda(\kappa_2)$ by solving (3.4a) numerically for fixed κ_2 and a range of temperatures β^{-1}. Thereby we determine the bifurcation point as a function of β, as $\lambda(\kappa_2)$ passes through zero.

4.0.2 Key for the Figures

In each solution figure we plot: the initial equilibrium density $\varrho(\mathbf{r})$ (black solid), the transient density $\varrho(\mathbf{r}, t)$ (red solid), and the stable density $\varrho(\mathbf{r}, t_*)$ (blue solid). In each right hand figure we plot the order parameter $\nu(\beta)$ (blue dots) and the minimum eigenvalue $\lambda(\kappa_2)$ (black dots) of (3.4a)–(3.4b).

4.0.3 Attractive Gaussian

The Gaussian kernel has been used as a constitutive model for the static two-body interaction for the dynamics of a population undergoing the transmission of an infectious disease (Grauer et al., 2020; Te Vrugt et al., 2020) as well as a simple model for the cell-cell forces influencing

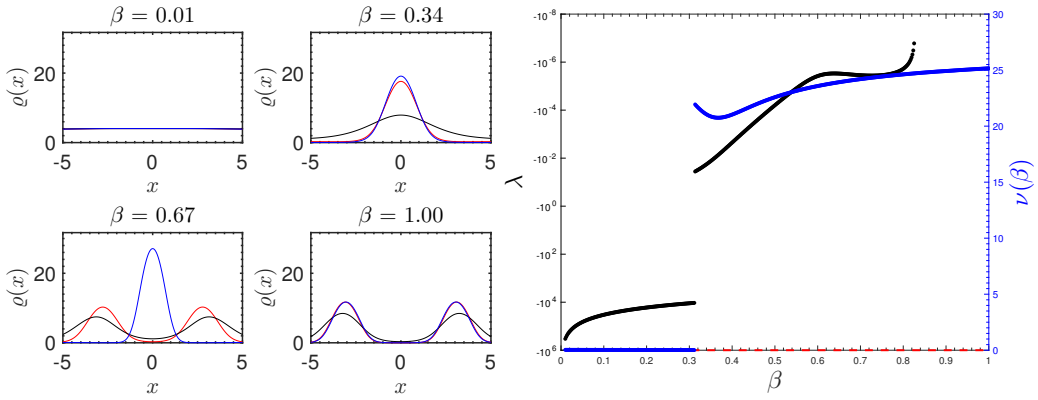

Figure 2: Plots of (a) initial equilibrium densities $\varrho(\mathbf{r})$ (black solid), transient density $\varrho(\mathbf{r}, t)$ (red solid), perturbation function $u(\mathbf{r})$ (magenta solid), final equilibrium $\varrho(\mathbf{r}, t_*)$ (blue solid) for the GEK kernel (4.4) $\{L, \kappa_2, \xi, N\} = \{5.0, 0.5, 1.9, 40\}$. (b) the minimum eigenvalue of (3.4a) (left, black solid) on a log scale, and the order parameter $\nu(\beta)$ with two solution branches: stable (right, blue solid) and unstable (red dashed).

the structure and dynamics of living tissues and tumour growth (Al-Saedi et al., 2018). We consider the Gaussian kernel, taking the form

$$V_2(x - x') = -e^{-(x-x')^2/(2\xi^2)}. \tag{4.3}$$

For the background field, we have chosen the trivial potential $V_1 \equiv 0$. We will consider the effects of background fields in later examples. Note that the choice of sign in (4.3) produces clustered densities. For small κ_2, this is confirmed by the dispersion relation (3.11), since the Fourier transform of a Gaussian is positive. The kernel (4.3) is short range and ξ acts as the attraction length. As such, the smaller ξ the larger the effective range of attraction. Figure 1a shows example equilibrium densities, as well as transient ones, with the choice of parameters provided in the caption. We see that initially for high temperatures the equilibrium density $\varrho(\mathbf{r})$ is stable to small perturbations and the transient density $\varrho(\mathbf{r}, t)$ (red line) quickly converges to $\varrho(\mathbf{r}, t_*) = \varrho(\mathbf{r})$.

For lower temperatures, as in the periodic case (c.f. Martzel & Aslangul (2001)), we find that stable n-peak solutions are possible (not shown), where $\varrho(\mathbf{r}, t_*) \neq \varrho(\mathbf{r})$. The number, n, of peaks increases with decreasing temperature, as do the density gradients, meaning more spectral collocation points are required to obtain a given solution accuracy. As such, the eigenvalue problem (3.4a)–(3.4b) becomes ever more computationally intractable as the number of density peaks increases. We find that the larger n-peak equilibrium densities are unstable against small perturbations, instead converging to stable, fewer-peaked distributions. Additionally, the annihilation of the peaks occurs through the absorption of weaker peaks (with relatively lower density) into strong peaks. In Figure (1b) we see the order parameter splits into two branches: stable solutions (blue solid) and unstable solutions (red dashed). The bifurcation point occurs at the critical inverse temperature $\beta_c = 0.329$, as confirmed by the density plot in 1a.

4.0.4 Generalised Exponential Kernel

In biology, tissue growth has been modelled by use of DDFTs in combination with Generalised Exponential Kernels (GEKs) accounting for the two-body interaction between tumour cells (Al-Saedi et al., 2018).

$$V_2(x - x') = -e^{-(x-x')^4/\xi^4} \tag{4.4}$$

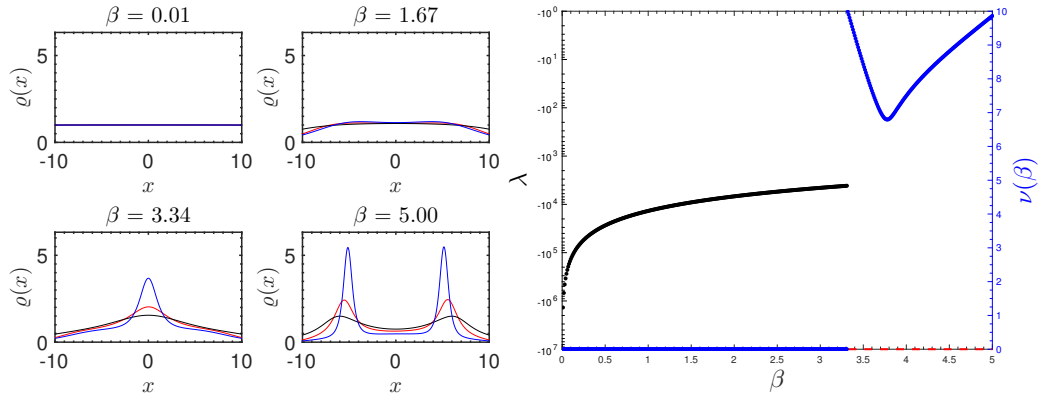

(a) (b)

Figure 3: Plots of (a) initial equilibrium densities $\varrho(\mathbf{r})$ (black solid), transient density $\varrho(\mathbf{r}, t)$ (red solid), perturbation function $u(\mathbf{r})$ (magenta solid), final equilibrium $\varrho(\mathbf{r}, t_*)$ (blue solid) for the Morse kernel (4.5) $\{L, \kappa_2, \xi, N\} = \{10.0, 0.3, 1.9, 20\}$. (b) the minimum eigenvalue of (3.4a) (left, black solid) on a log scale, and the order parameter $\nu(\beta)$ with two solution branches: stable (right, blue solid) and unstable (red dashed).

where we have chosen pure attraction. The value of ξ may be tuned according to both the biological characteristics of the swarming species and volume of the system. For the background field, we have once again chosen the trivial potential $V_1 \equiv 0$. In Figure 3a we show that the equilibrium densities $\varrho(\mathbf{r})$ vary from the Gaussian case. For sufficiently low temperatures strengths, bimodal densities are stable, differing to the Gaussian case. Nucleation occurs at an inhomogeneity, in this case, at the boundary. This is justified from a physical standpoint, that a particle near this boundary is pulled from one side only, differing from that of a particle located in the bulk. Such a phenomenon is characteristic of the boundary condition choice. Here, we see that the bifurcation point occurs at a slightly higher temperature compared to the Gaussian case, namely $\beta_c = 0.308$.

4.0.5 Morse Model for Swarming Agents

The Morse kernel is an example of a short range potential force in individual based models of swarming systems (see, e.g.,D'Orsogna et al. (2006); Mogilner et al. (2003))

$$V_2(x - x') = -e^{-|x-x'|/\xi} \tag{4.5}$$

where we have chosen pure attraction. The value of ξ may be tuned according to both the biological characteristics of the swarming species and volume of the system. Focussing once again on the effect of the order of the exponential kernel, for the background field, we have again chosen the trivial potential $V_1 \equiv 0$. In Figure 3a we show that the equilibrium densities $\varrho(\mathbf{r})$ vary dramatically from the Gaussian and generalised cases. At higher temperatures, there is slight disagreement between $\varrho(\mathbf{r})$ (black) and $\varrho(\mathbf{r}, t_*)$, attributable to the fact that the numerical termination time t_* is necessarily finite. For sufficiently low temperatures, sharper density profiles may arise, e.g., the 'Schloss' shape occurring at $\beta = 5.0$, as confirmed in the bifurcation diagram Figure 3b.

For both the Gaussian (4.3) and Morse (4.5) kernels we provide the second variation of the free energy $\delta^2\mathcal{F}[\varrho]$, evaluated at the eigenfuncion w associated to the minimum eigenvalue of (3.4a)–(3.4b), in each case. We observe that $\delta^2\mathcal{F}[\varrho]$ becomes negative for both examples, coinciding with the critical inverse temperatures β_c computed in both respective examples, indicating that the density field is unstable at those temperatures.

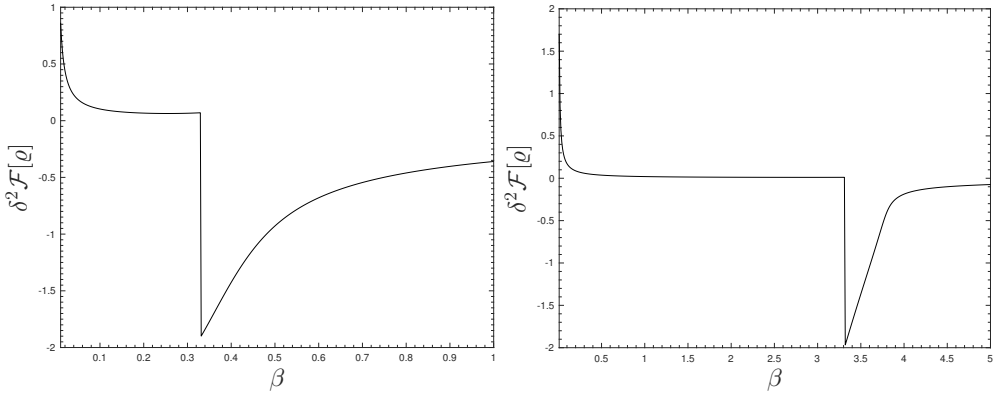

(a) (b)

Figure 4: Plots of the second variation of the free energy $\delta^2\mathcal{F}[\varrho]$ for (a) the Gaussian kernel (4.3) and (b) the Morse kernel (4.5), both evaluated using the eigenfunction w associated to the minimum eigenvalue solving (3.4a)–(3.4b).

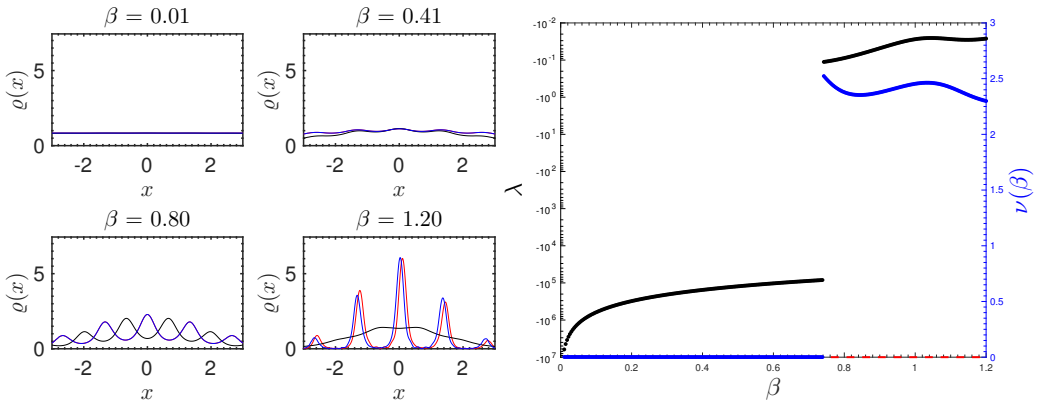

(a) (b)

Figure 5: Plots of (a) initial equilibrium densities $\varrho(\mathbf{r})$ (black solid), transient density $\varrho(\mathbf{r}, t)$ (red solid), perturbation function $u(\mathbf{r})$ (magenta solid), final equilibrium $\varrho(\mathbf{r}, t_*)$ (blue solid) for the Onsager kernel (4.6) $\{L, \kappa_1, \kappa_2, \xi_2, N\} = \{3.0, 0.05, 1.1, 0.9, 5\}$. (b) the minimum eigenvalue of (3.4a) (left, black solid) on a log scale, and the order parameter $\nu(\beta)$ with two solution branches: stable (right, blue solid) and unstable (red dashed).

4.0.6 Onsager Model for Liquid Crystals

In this section we consider equilibrium states such as those found in models of alignment in liquid crystals (De Gennes & Prost, 1993; Onsager, 1949). The two-body kernel is given by

$$V_2(x - x') = |\sin(\tfrac{2\pi}{L\xi}(x - x'))|. \tag{4.6}$$

This time we include a one-body force to modulate the interparticle forces by choosing a quadratic potential of the form

$$V_1(x) = \kappa_1 x^2.$$

In Figure 5a we show the liquid crystal becomes unstable against mean-zero perturbations. We see that, as temperature is lowered, the equilibrium densities with many $n-$peaks converge to an $N-$peak distribution. Once again, at higher temperatures, there is slight

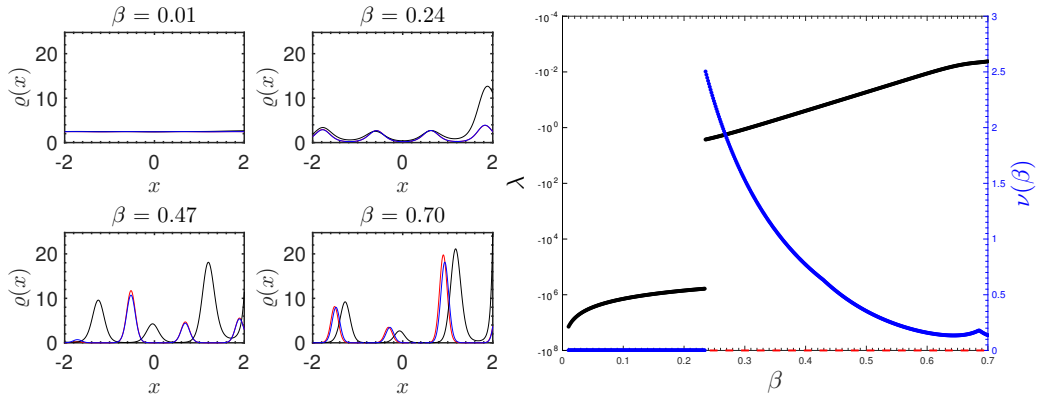

(a) (b)

Figure 6: Plots of (a) initial equilibrium densities $\varrho(\mathbf{r})$ (black solid), transient density $\varrho(\mathbf{r}, t)$ (red solid), perturbation function $u(\mathbf{r})$ (magenta solid), final equilibrium $\varrho(\mathbf{r}, t_*)$ (blue solid) for the Kuramoto kernel (4.7) $\{L, \kappa_1, \kappa_2, \xi_1, \xi_2, N\} = \{2.0, 2.0, 0.8, 1.0, 0.6, 10\}$. (b) the minimum eigenvalue of (3.4a) (left, black solid) on a log scale, and the order parameter $\nu(\beta)$ with two solution branches: stable (right, blue solid) and unstable (red dashed).

disagreement between $\varrho(\mathbf{r})$ (black) and $\varrho(\mathbf{r}, t_*)$, attributable to the fact that the numerical termination time t_* is necessarily finite. In Figure 5b we show the bifurcation occurring at the critical inverse temperature $\beta_c = 0.738$, confirmed by the behaviour of the second variation of the free energy in 7a.

4.0.7 Uneven Noisy Kuramoto

The Noisy Kuramoto system models the synchronisation of noisy oscillators interacting through their phases (Acebrón et al., 2005; Kuramoto, 1981). It is also known by the 'cosine model' has been considered for the examination of clustering in continuum models of many-body systems (Battle, 1977; Messer & Spohn, 1982). Here we choose

$$V_2(x - x') = -\cos \tfrac{2\pi}{L\xi}(x - x'), \tag{4.7}$$

with a manifestly uneven background potential of the form

$$V_1(x) = ax^2(x - c^{-1})(2x + c^{-1}).$$

In Figure 6a we chose $a = 0.05$, $c = ab$ and $b = 1.0$. In this case we see that for sufficiently low temperatures, the uniform density is unstable against small perturbations, and converges to uneven-$n-$peak densities. This is concurrent with the physical viewpoint, that for a low enough temperature - equivalently high enough oscillation magnitude κ_2 - the particles begin to resonate. This is in contrast to, for example, the relation to fewer peaks phenomena observed in the exponential models. In Figure 6b we show the bifurcation occurring at $\beta_c = 0.234$, confirmed by the behaviour of $\nu(\kappa_2)$ and $\lambda(\kappa_2)$. We note that the equilibrium density profiles and bifurcation diagram obtained in this example can not be otherwise analytically derived from Fourier methods, most notably because the equilibrium densities are demonstrably non-periodic.

Finally, in Figure 7 we plot the second variation of the free energy $\delta^2\mathcal{F}[\varrho]$ for both the Onsager (4.6) and Kuramoto (4.7) cases. We note that positivity is preserved in both cases. This is a numerical artefact of the Picard scheme used to compute the equilibrium densities in (4.1a)–(4.1b) close to the bifurcation point. In particular, at the critical inverse temperature, the error at each iteration level numerically perturbs the solution away from

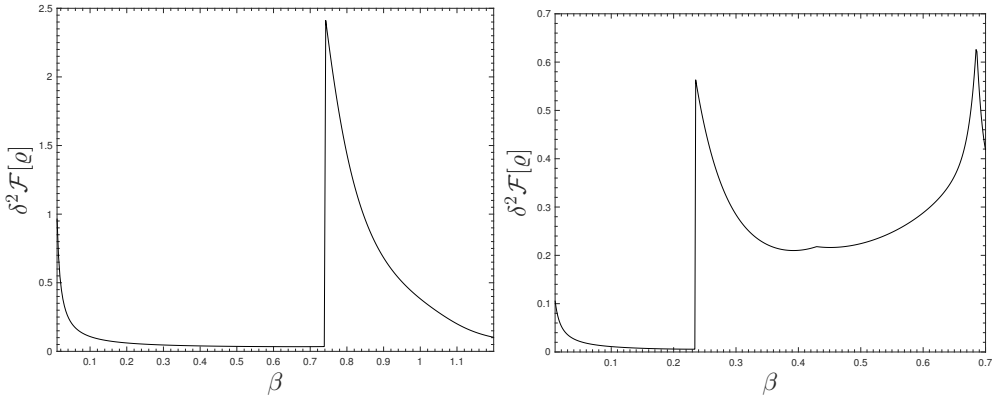

(a) (b)

Figure 7: Plots of the second variation of the free energy $\delta^2\mathcal{F}[\varrho]$ for (a) the Onsager kernel (4.6) and (b) the Kuramoto kernel (4.7), both evaluated using the eigenfunction w associated to the minimum eigenvalue solving (3.4a)–(3.4b).

the (unstable) density profile, causing the scheme to converge on the nearest stable densities profile. Nonetheless the discontinuity in the derivative of $\delta^2\mathcal{F}[\varrho]$ with respect to β indicates the bifurcation point and is consistent with the behaviour of the minimum eigenvalue and order parameter in both cases (c.f. Figures 5b, 6b).

5 Discussion

We have performed a linear stability analysis of the mean field Fokker–Planck equation subject to a nonlinear no-flux boundary condition. This required an analysis of the spectral properties of the linearised operator $\mathcal{L}_\varrho$. We showed that, due to the choice of boundary condition and inclusion of one-body forces, the spectrum of $\mathcal{L}_\varrho$ differs considerably compared to standard problems with periodic boundary conditions. However, by use of a formal perturbation expansion, we showed that the dispersion relation for the smallest of eigenvalue of $\mathcal{L}_\varrho$ is equivalent to the one in the periodic case, in the limit of weak two-body interactions and with no background field. This result in d dimensions, and general to the choice of V_2, is consistent with previous studies, e.g. Chavanis (2014); Chavanis et al. (2005), where the eigenvalue problem is solved in 1D for a specific choice of V_2.

In the most general case, for order unity two-body interactions in the presence of an additional confining potential, we have provided numerical solutions to full the eigenvalue problem which expands on previous studies of the mean field Fokker–Planck equation for conserved mass systems, e.g.,(Martzel & Aslangul, 2001). Thus the stability of non-periodic systems has been studied, as well as a wider class of two-body inter-particle potentials.

Additionally, we have established positivity and regularity of the equilibrium densities in Proposition 1 and established the first general bifurcation theory for conserved mass systems in Theorem 2. The assumptions involved in establishing these results are in line with physically realistic applications of complex, particles systems. There are many promising extensions to both the theory and numerical analysis presented here, including: the extension of linear stability analysis to hard core fluids as found in the DFT community (including anisotropic particles, self-motile particles), numerical computations in higher dimensions, the stability analysis of inertial dynamics as well as stability in the presence of non-zero non-homogeneous solvent flows.

Acknowledgements

BDG would like to acknowledge support from EPSRC EP/L025159/1. RDMW is grateful to EPSRC for PhD funding. GAP was supported by the EPSRC through grant numbers EP/P031587/1, EP/L024926/1, and EP/L020564/1. This research was funded in part by JPMorgan Chase & Co. Any views or opinions expressed herein are solely those of the authors listed, and may differ from the views and opinions expressed by JPMorgan Chase & Co. or its affiliates. This material is not a product of the Research Department of J.P. Morgan Securities LLC. This material does not constitute a solicitation or offer in any jurisdiction.

A Characterisation of Equilibrium States

We denote by $P(\Omega)$ as the space of Borel probability density measures on Ω, by $P_{ac}(\Omega)$ the subset of $P(\Omega)$ containing absolutely continuous probability density measures (with respect to the Lebesgue measure), and by $P_{ac}^{+}(\Omega)$ the subset of $P_{ac}(\Omega)$ having strictly positive densities almost everywhere.

Proposition 1 (Existence, Regularity, and Strict Positivity of Equilibrium Densities)**.** *Without loss of generality let* $\int \mathrm{d}\mathbf{r}\, \varrho(\mathbf{r}) = 1$*. Let*

$$V_1, V_2 \in H^1(\Omega) \cap L^\infty(\Omega), \tag{A.1}$$

and consider the stationary problem (2.5)*. Then we have that*

1. *There exists a weak solution* $\varrho \in H^1(\Omega) \cap P_{ac}(\Omega)$ *to* (2.5) *as a fixed point of the equation* (2.6)*.*
2. *Any weak solution* $\varrho \in H^1(\Omega) \cap P_{ac}(\Omega)$ *is smooth and strictly positive, that is* $\varrho \in C^\infty(\bar{\Omega}) \cap P_{ac}^{+}(\Omega)$*.*

Proof. The proof is similar to (Carrillo et al., 2019, Theorem 2.3) but one must check the conclusions of the theorem hold with no flux boundary conditions and a confining potential V_1. The weak formulation of (2.5) is

$$-\int \mathrm{d}\mathbf{r}\, \nabla_{\mathbf{r}}\eta \cdot \nabla_{\mathbf{r}}\varrho - \int \mathrm{d}\mathbf{r}\, \nabla_{\mathbf{r}}\eta \cdot \varrho \nabla_{\mathbf{r}} V_1 - \kappa_2 \int \mathrm{d}\mathbf{r}\, \nabla_{\mathbf{r}}\eta \cdot \varrho \nabla_{\mathbf{r}} V_2 \star \varrho = 0, \tag{A.2}$$

for $\eta \in H^1(\Omega)$ where we have used the no-flux boundary condition in (2.5) on ϱ and we seek solutions $\varrho \in H^1(\Omega) \cap P_{ac}(\Omega)$. Now define $\mathcal{T} : P_{ac}(\Omega) \to P_{ac}(\Omega)$ by

$$\begin{aligned} \mathcal{T}\varrho &= \frac{1}{Z(\varrho, \kappa_2)} e^{-(V_1 + \kappa_2 V_2 \star \varrho)}, \\ Z(\varrho, \kappa_2) &= \int \mathrm{d}\mathbf{r}\, e^{-(V_1 + \kappa_2 V_2 \star \varrho)}. \end{aligned} \tag{A.3}$$

By (2.6) we see that

$$\|\mathcal{T}\varrho\|_{L^2(\Omega)}^2 \leq \frac{1}{|\Omega|} e^{4(|||V_1\|_{L^\infty(\Omega)} + |\kappa_2| \|V_2\|_{L^\infty(\Omega)})} =: E_0, \tag{A.4}$$

and therefore we seek solutions to (2.6) in the set $E := \{\varrho \in L^2(\Omega) : \|\varrho\|_{L^2(\Omega)}^2 \leq E_0\}$. Note that E is a closed, convex subset of $L^2(\Omega)$ and therefore we may redefine T to act on E. Additionally we see that for $\varrho \in E$

$$\|\mathcal{T}\varrho\|_{H^1(\Omega)}^2 = \|\mathcal{T}\varrho\|_{L^2(\Omega)}^2 + \|\nabla_{\mathbf{r}} T\varrho\|_{L^2(\Omega)}^2 \leq E_0 \left(1 + 2\|\nabla V_1\|_{L^2(\Omega)}^2 + |\kappa_2|^2 \|\nabla V_2\|_{L^2(\Omega)}^2 E_0\right), \tag{A.5}$$

where we have used that $\varrho \in L^1(\Omega)$ (Dressler, 1987, Theorem 1) and $V_1, V_2 \in H^1(\Omega)$. Similarly to (Carrillo et al., 2019, Theorem 2.3) we have by (A.4) that $\mathcal{T}(E) \subset E$ and by (A.5) $\mathcal{T}(E)$ is uniformly bounded in $H^1(\Omega)$. Therefore by Rellich's Compactness Theorem, $\mathcal{T}(E)$ is relatively compact in $L^2(\Omega)$, and therefore in E, since E is closed.

We may show using similar calculations to (Dressler, 1987, Theorem 1) that the nonlinear map $\mathcal{T}$ is Lipschitz continuous in E, and by Schauder Fixed Point Theorem there exists $\varrho \in E$ solving (2.6) which by (A.5) is in $H^1(\Omega)$. By inserting the expression for $\mathcal{T}\varrho$ (A.3) into (A.2) we obtain statement (1.). Also note that solutions $\varrho \in E$ to (2.6) are bounded below by $E_0^{-1}/|\Omega|^2$ giving positivity of solutions.

We now show that every weak solution in $\varrho \in H^1(\Omega) \cap P_{ac}(\Omega)$ is a fixed point of the nonlinear map in (2.6). Consider the frozen weak formulation

$$-\int \mathrm{d}\mathbf{r}\, \nabla_{\mathbf{r}}\eta \cdot \nabla_{\mathbf{r}}\theta - \kappa_1 \int \mathrm{d}\mathbf{r}\, \nabla_{\mathbf{r}}\eta \cdot \nabla_{\mathbf{r}} V_1 \theta - \kappa_2 \int \mathrm{d}\mathbf{r}\, \nabla_{\mathbf{r}}\eta \cdot \nabla_{\mathbf{r}} V_2 \star \varrho\, \theta = 0. \tag{A.6}$$

This is the weak formulation of the PDE (for the unknown function θ)

$$\begin{aligned} \nabla_{\mathbf{r}} \cdot (\nabla_{\mathbf{r}}\theta + \theta(\nabla_{\mathbf{r}} V_1 + \nabla_{\mathbf{r}} V_2 \star \varrho)) = 0, \\ \text{s.t.} \quad \nabla_{\mathbf{r}} \left((\mathcal{T}\varrho)^{-1}\theta \right) \cdot \mathbf{n}|_{\partial\Omega} = 0. \end{aligned}$$

We note that we may rewrite the weak formulation (A.6) as

$$-\int \mathrm{d}\mathbf{r}\, \nabla_{\mathbf{r}}\eta \cdot \nabla_{\mathbf{r}} h\, \mathcal{T}\varrho = 0$$

for every $\eta \in H^1(\Omega)$ and where $h = \theta/(\mathcal{T}\varrho)$. This holds true for any η, in particular $\eta = h$ hence we find

$$-\int \mathrm{d}\mathbf{r} \left| (\mathcal{T}\varrho)^{1/2} \nabla_{\mathbf{r}} h \right|^2 = 0$$

where we have used that fact that $\mathcal{T}\varrho$ is strictly positive. All in all we obtain $\nabla_{\mathbf{r}} h = 0$ a.e. and hence $\theta = \mathcal{T}\varrho$ up to normalisation (fixed by the number of particles N). Hence we must have $\theta \equiv \mathcal{T}\varrho$ and we conclude that since $\varrho = \mathcal{T}\varrho$, any weak solution $\varrho \in H^1(\Omega) \cap P^+_{ac}(\Omega)$ of (A.2) must be such that $\varrho = \mathcal{T}\varrho$. The regularity of ϱ follows from the same bootstrapping argument of (Carrillo et al., 2019, Theorem 2.3). □

B Results for Bifurcation Theory

In this section we present analytical results for the bifurcation theory to accompany the linear stability analysis of Section 3. The following results are an extension of standard theory (Carrillo et al., 2019; Crandall & Rabinowitz, 1971), which is usually applied to systems with periodic boundary conditions in which the so called 'liquid state' (for κ_2 sufficiently small, or equivalently inverse temperature β sufficiently small) corresponds to the uniform distribution. For our systems, with vanishing flux $\mathbf{j}|_{\partial\Omega} \cdot \mathbf{n} = 0$, the corresponding equilibrium state is not, except in very special circumstances, uniform. Therefore we must check the conditions of the bifurcation theory for non constant equilibria.

We start by computing the first few Frechet derivatives of the map $F(\varrho, \kappa)$ defined in (B.4) in variations $w_1(\mathbf{r};\kappa_2)$, $w_2(\mathbf{r};\kappa_2)$, $w_3(\mathbf{r};\kappa_2) \in L^2(\Omega)$, the eigenfunctions of $\mathcal{L}_\varrho$ which will be be useful for the proceeding theorem. We have that

$$\begin{aligned} D_\varrho F(\varrho, \kappa_2)[w_1(\mathbf{r};\kappa_2)](\mathbf{r}) &= w_1(\mathbf{r};\kappa_2) + \kappa_2 \varrho V_2 \star w_1(\mathbf{r};\kappa_2) - \kappa_2 \varrho \int \mathrm{d}\mathbf{r} \varrho V_2 \star w_1(\mathbf{r};\kappa_2) \\ D_\kappa F(\varrho, \kappa_2)(\mathbf{r}) &= \varrho V_2 \star \varrho - \varrho \int \mathrm{d}\mathbf{r}\, \varrho V_2 \star \varrho, \end{aligned} \tag{B.1}$$

$$
\begin{aligned}
D^2_{\varrho\,\kappa}F\left(\varrho,\kappa_2\right)\left[w_1(\mathbf{r};\kappa_2)\right](\mathbf{r}) &= \varrho V_2 \star w_1(\mathbf{r};\kappa_2) - \varrho\int \mathrm{d}\mathbf{r}\,\varrho V_2 \star w_1(\mathbf{r};\kappa_2)\\
&\quad + D_\varrho F\left(\varrho,\kappa_2\right)\left[w_1(\mathbf{r};\kappa_2)\right](\mathbf{r}) V_2 \star \varrho\\
&\quad - D_\varrho F\left(\varrho,\kappa_2\right)\left[w_1(\mathbf{r};\kappa_2)\right](\mathbf{r})\int \mathrm{d}\mathbf{r}\,\varrho V_2 \star \varrho\\
&\quad - \varrho\int \mathrm{d}\mathbf{r}\, D_\varrho F\left(\varrho,\kappa_2\right) V_2 \star \varrho, \qquad \text{(B.2)}
\end{aligned}
$$

$$
\begin{aligned}
&D^2_{\varrho\,\varrho}F\left(\varrho,\kappa_2\right)\left[w_1(\mathbf{r};\kappa_2), w_2(\mathbf{r};\kappa_2)\right](\mathbf{r})\\
&\quad = \kappa_2\left(w_2(\mathbf{r};\kappa_2) - D_\varrho F\left(\varrho,\kappa_2\right)\left[w_2(\mathbf{r};\kappa_2)\right]\right) V_2 \star w_1(\mathbf{r};\kappa_2) - \kappa_2\left(w_2(\mathbf{r};\kappa_2)\right.\\
&\qquad \left. - D_\varrho F\left(\varrho,\kappa_2\right)\left[w_2(\mathbf{r};\kappa_2)\right]\right)\int \mathrm{d}\mathbf{r}\,\varrho V_2 \star w_1(\mathbf{r};\kappa_2)\\
&\qquad - \kappa_2\varrho\int \mathrm{d}\mathbf{r}\,\left(w_2(\mathbf{r};\kappa_2) - D_\varrho F\left(\varrho,\kappa_2\right)\left[w_2(\mathbf{r};\kappa_2)\right]\right) V_2 \star w_1(\mathbf{r};\kappa_2). \qquad \text{(B.3)}
\end{aligned}
$$

Note that the Frechet derivatives (B.1),(B.3) differ from those (Carrillo et al., 2019, Equations (4.3)–(4.6)) owing to the non-constant equilibrium density ϱ.

Theorem 2. *Let $F : L^2(\Omega)\times\mathbb{R} \to L^2(\Omega)$ be a twice Fréchet differentiable mapping defined as*

$$
F(\varrho,\kappa_2) = \varrho - \frac{1}{Z(\varrho,\kappa_2)} e^{-(\kappa_1 V_1 + \kappa_2 V_2 \star \varrho)}, \qquad \text{(B.4)}
$$

where $Z(\varrho,\kappa_2) = \int \mathrm{d}\mathbf{r}\, e^{-(\kappa_1 V_1 + \kappa_2 V_2\star\varrho)}$. Additionally, let V_2 satisfy Assumption (A.1) *and assume there exists a critical wave number $n = k^\sharp$ of the eigenvalue problem* (3.4a)–(3.4b)*, such that a zero eigenvalue exists at a critical interaction strength $\kappa_2^\sharp$. Let the following hold:*

1. *$K = \ker D_\varrho F(\varrho_{\kappa_2^\sharp},\kappa_2^\sharp)$, $R = \operatorname{Im} D_\varrho F(\varrho_{\kappa_2^\sharp},\kappa_2^\sharp)$, where $(\varrho_{\kappa_2^\sharp},\kappa_2^\sharp) \in L^2(\Omega)\times\mathbb{R}$ with $F(\varrho_{\kappa_2^\sharp},\kappa_2^\sharp) = 0$.*
2. *Let $D_\varrho F(\varrho_{\kappa_2^\sharp},\kappa_2^\sharp)$ be a Fredholm operator with $\operatorname{ind} D_\varrho F(\varrho_{\kappa_2^\sharp},\kappa_2^\sharp) = 0$ and $\dim K = 1$.*
3. *Let $X_0 := \left\{\phi \in L^2(\Omega) : \langle v_0,\phi\rangle_{L^2} = 0\right\} \subset L^2(\Omega)$ with $L^2(\Omega) = K \oplus X_0$, for $K = \operatorname{span}\{v_0\}$, for some $v_0 \in L^2(\Omega)$.*

Then there exists a neighbourhood $U\times V \subset L^2(\Omega)\times\mathbb{R}$ and a unique, continuously differentiable function $\Psi : U\cap K \times V \to W$, with $w = \Psi(v,\kappa_2)$ for $w \in W = U\cap X_0$, $v \in U\cap K$, $\kappa_2 \in V$ and $W = U\cap X_0$, such that:

- *$(\varrho_{\kappa_2^\sharp},\kappa_2^\sharp)$ is a bifurcation point of $F(\varrho,\kappa_2) = 0$,*
- *there exists a branch of solutions to $F(\varrho_*(\mathbf{r};s),\kappa_2(s)) = 0$ of the form*

$$
\varrho_*(\mathbf{r};s) = \varrho_{\kappa_2^\sharp} + s w_{k^\sharp}(\mathbf{r};\kappa_2^\sharp) + \Psi(s w_{k^\sharp}(\mathbf{r};\kappa_2^\sharp),\kappa_2(s)), \qquad \text{(B.5)}
$$

and where $w_{k^\sharp}(\mathbf{r};\kappa_2^\sharp) \in \ker D_\varrho F(\varrho_{\kappa_2^\sharp},\kappa_2^\sharp)\cap L^2(\Omega)$ is the critical eigenfunction of $\mathcal{L}_\varrho$ associated to the critical wave number $k^\sharp$, $s \in (-\delta,\delta)$ for some $\delta > 0$, and $\kappa_2 : (-\delta,\delta) \to V$ is a twice differentiable function in a neighbourhood V of $\kappa_2^\sharp$ with $\kappa_2(0) = \kappa_2^\sharp$.

Proof. We show that the Crandall–Rabinowitz Theorem holds, in particular that there exists $\kappa_2^\sharp \in \mathbb{R}$ such that

$D_\varrho(\varrho_{\kappa_2^\sharp},\kappa_2^\sharp)$ is a Fredholm operator with index zero and has a one-dimensional kernel.

$D^2_{\varrho\,\kappa}(\varrho_{\kappa_2^\sharp}, \kappa_2^\sharp)[w_0(\mathbf{r};\kappa_2)] \notin \mathrm{Im}\left(D_\varrho(\varrho_{\kappa_2^\sharp}, \kappa_2^\sharp)\right)$, where $w_0(\mathbf{r};\kappa_2) \in \ker\left(D_\varrho(\varrho_{\kappa_2^\sharp}, \kappa_2^\sharp)\right)$,

and $\|w_0(\cdot;\kappa_2)\|_{L^2_{\varrho^{-1}}} = 1$. The proof is similar to (Carrillo et al., 2019, Theorem 1.2) but we check the conditions hold for the spectrum of $\mathcal{L}_\varrho$, which differs when compared with periodic equilibria. First we rewrite $D_\varrho F$ in (B.1) as

$$D_\varrho F = \boldsymbol{I} - \kappa_2 T$$

where $T : L^2(\Omega) \to L^2(\Omega)$ is defined for $w^{(\kappa_2)} \in L^2(\Omega)$ by

$$(Tw^{(\kappa_2)})(\mathbf{r}) = -\varrho V_2 \star w(\mathbf{r};\kappa_2) + \varrho \int \mathrm{d}\mathbf{r}\, \varrho V_2 \star w(\cdot;\kappa_2)(\mathbf{r}).$$

Using this definition we show that T is a Hilbert-Schmidt operator. In particular we have that the kernel $-\varrho V_2 \star (\cdot) + \varrho \int \mathrm{d}\mathbf{r}\, \varrho V_2 \star (\cdot)$ is square integrable on with respect to $\varrho^{-1}_{\kappa_2}$ on $\bar{\Omega} \subset \mathbb{R}$, by using Assumption (A.1) on V_2, and hence is a compact Hilbert Schmidt operator. Therefore, $\boldsymbol{I} - \kappa_2 T$ is Fredholm by (Davies, 2007, Corollary 4.3.8). Additionally, we see that the mapping $\kappa_2 :\to \boldsymbol{I} - \kappa_2 T$ is norm continuous:

$$\|\boldsymbol{I} - \kappa_{2_1} T - \boldsymbol{I} + \kappa_{2_2} T\| = |\kappa_{2_1} - \kappa_{2_2}| \|T\|.$$

Then, since the index of a Fredholm operator is homotopy invariant (Davies, 2007, Corollary 4.3.8), we have $\mathrm{ind}\,(\boldsymbol{I} - \kappa_2 T) = \mathrm{ind}(\boldsymbol{I}) = 0$. We now diagonalise $\boldsymbol{I} - \kappa_2 T$ with respect to $\{\lambda_k, w_k(\cdot;\kappa_2)\}$. Before we do this we factorise $\mathcal{L}_\varrho$ into the product

$$\mathcal{L}_\varrho = \mathcal{A}_\varrho \left(\mathbf{1} - \kappa_2 T^*\right), \tag{B.6}$$

where

$$\mathcal{A}_\varrho w := \nabla \cdot \left(\varrho \nabla \left(\varrho^{-1} w\right)\right),$$

The explicit form of the operator T^* is readily derived as, for $u \in L^2(\Omega, \varrho^{-1})$ mean zero,

$$\begin{aligned}\langle u, Tw(\cdot;\kappa_2)\rangle_{L^2_{\varrho^{-1}}} &= \int \mathrm{d}\mathbf{r}\, \varrho^{-1} u(\mathbf{r}) \left(-\varrho V_2 \star w(\cdot;\kappa_2)(\mathbf{r}) + \varrho \int \mathrm{d}\mathbf{z}\, \varrho V_2 \star w(\cdot;\kappa_2)(\mathbf{z})\right) \\ &= -\int \mathrm{d}\mathbf{r}'\, \varrho^{-1} \varrho w(\mathbf{r}';\kappa_2) V_2 \star u(\mathbf{r}') + \int \mathrm{d}\mathbf{r}'\, w(\mathbf{r}';\kappa_2) V_2 \star \varrho(\mathbf{r}') \int \mathrm{d}\mathbf{r}\, u(\mathbf{r}).\end{aligned}$$

The second integral vanishes because u is mean zero, and hence we find

$$T^* u = -\varrho V_2 \star u,$$

and by comparing with definition (3.2), the factorisation (B.6) is verified. With this factorisation, we obtain

$$(\boldsymbol{I} - \kappa_2 T)\, w_k(\mathbf{r};\kappa_2) = \lambda_k \left(\mathcal{A}_\varrho^{-1}\right)^* w_k(\mathbf{r};\kappa_2).$$

Now we see that if $\kappa_2 = \kappa_2^\sharp$ is chosen such that $\lambda_{k^\sharp} = 0$ (the right most branch before crossing the κ_2 axis) then $\dim\left(\ker\left(\boldsymbol{I} - \kappa_2 T\right)\right) = 1$ for $\kappa_2 = \kappa_2^\sharp$ and Condition ? is satisfied.

Now since $\mathrm{Im}\left(\boldsymbol{I} - \kappa_2 T\right)$ is closed we have that $\mathrm{Im}\left(\boldsymbol{I} - \kappa_2 T\right) = \ker\left(\boldsymbol{I} - \kappa_2 T^*\right)^\perp$ where T^* is the adjoint of T. Now let $v_0 \in \ker\left(\mathbf{1} - \kappa_2 T\right)$, $v_0 \not\equiv 0$, then

$$v_0 + \kappa_2 \varrho V_2 \star v_0 + \kappa_2 \varrho \int \mathrm{d}\mathbf{z}\, \varrho V_2 \star v_0 = 0. \tag{B.7}$$

Now by integrating (B.7) over $\mathbf{r} \in \Omega$ we observe

$$0 + \kappa_2 \int \mathrm{d}\mathbf{r}\, \varrho V_2 \star v_0 + \kappa_2 \int \mathrm{d}\mathbf{r}\, \varrho \left(\int \mathrm{d}\mathbf{z}\, \varrho V_2 \star v_0\right) = 0,$$

and therefore

$$c_0(1+N)=0,$$

where $c_0=\int \mathrm{d}\mathbf{r}\,\varrho V_2\star v_0$ and $N=\int \mathrm{d}\mathbf{r}\,\varrho$, and we must have that $c_0\equiv 0$. Hence we see that if $v_0\in\ker\left(\mathbf{1}-\kappa_2 T\right)$ then $v_0\in\ker\left(\mathbf{1}-\kappa_2 T^*\right)$.

Now using by using the formula (B.2), evaluated at the variation $w_1(\mathbf{r};\kappa_2)=v_0$ we find,

$$\langle D^2_{\varrho\,\kappa}F\left(\varrho,\kappa_2\right)[v_0],v_0\rangle_{L^2_{\varrho^{-1}}}=-\langle Tv_0,v_0\rangle_{L^2_{\varrho^{-1}}}=-\kappa_2^{-1}\|v_0\|^2_{L^2_{\varrho^{-1}}}\neq 0,$$

since $v_0\neq 0$ by assumption. This implies that $D^2_{\varrho\,\kappa}F\left(\varrho,\kappa_2\right)[v_0]\notin\ker\left(\boldsymbol{I}-\kappa_2 T^*\right)^{\perp}$. Therefore Condition ? is satisfied. We now apply the Crandall-Rabinowitz Theorem (Carrillo et al., 2019, Theorem A.2) to obtain (B.5). □

This is the strongest result on the nature of the curve $(\varrho_*(\mathbf{r};s),\,\kappa_2(s))\subset\mathbb{R}^2$ that we obtain, principally because we have that $D_\kappa F(\varrho,\kappa_2)\neq 0$ due to the fact that ϱ is not (in general) constant and hence we do not have the explicit form for the remainder term $r_1(s\,v_0,\psi(s))$ as in (Carrillo et al., 2019, Theorem 4.2)). Additionally, we do not show that $\kappa_2'(0)=0$ or $\kappa_2''(0)>0$ (and analogous results (Carrillo et al., 2019, Theorem 4.2) etc.) similarly because ϱ is not necessarily constant, and need not be an even function due to the presence of an external potential V_1.

References

Acebrón, J. A., Bonilla, L. L., Vicente, C. J. P., Ritort, F. & Spigler, R. (2005) The Kuramoto model: A simple paradigm for synchronization phenomena. *Rev. Mod. Phys*, **77**(1), 137. 4.0.7

Al-Saedi, H. M., Archer, A. J. & Ward, J. (2018) Dynamical density-functional-theory-based modeling of tissue dynamics: Application to tumor growth. *Phys. Rev. E*, **98**(2), 022407. 4.0.3, 4.0.4

Archer, A. J. & Evans, R. (2004) Dynamical density functional theory and its application to spinodal decomposition. *J. Chem. Phys.*, **121**(9), 4246–4254. 2

Barré, J., Degond, P. & Zatorska, E. (2017) Kinetic theory of particle interactions mediated by dynamical networks. *Multiscale Modeling & Simulation*, **15**(3), 1294–1323. 1

Battle, G. A. (1977) Phase transitions for a continuous system of classical particles in a box. *Commun. Math. Phys.*, **55**(3), 299–315. 4.0.7

Bertini, L., Giacomin, G. & Pakdaman, K. (2010) Dynamical aspects of mean field plane rotators and the Kuramoto model. *J. Stat. Phys.*, **138**(1), 270–290. 3

Bouchut, F. & Dolbeault, J. (1995) On long time asymptotics of the Vlasov-Fokker-Planck equation and of the Vlasov-Poisson-Fokker-Planck system with Coulombic and Newtonian potentials. *Differ. Integral Equ.*, **8**(3), 487–514. 2

Carrillo, J. A., Gvalani, R. S., Pavliotis, G. A. & Schlichting, A. (2018) Long-time behaviour and phase transitions for the McKean–Vlasov equation on the torus. *arXiv preprint arXiv:1806.01719*. 3.1.1

Carrillo, J. A., Gvalani, R. S., Pavliotis, G. A. & Schlichting, A. (2019) Long-Time Behaviour and Phase Transitions for the Mckean-Vlasov Equation on the Torus. *Arch, Rational Mech, Anal.* 1, 3, 3.2, 4.0.1, A, A, A, B, B, B, B

Chavanis, P.-H. (2014) The Brownian mean field model. *Eur. Phys. J. B*, **87**(5), 1–33. 3.1, 5

Chavanis, P.-H., Vatteville, J. & Bouchet, F. (2005) Dynamics and thermodynamics of a simple model similar to self-gravitating systems: the HMF model. *Eur. Phys. J. B*, **46**(1), 61–99. 3.1, 5

Chayes, L. & Panferov, V. (2010) The McKean–Vlasov equation in finite volume. *J. Stat. Phys.*, **138**(1-3), 351–380. 1

Chazelle, B., Jiu, Q., Li, Q. & Wang, C. (2017) Well-posedness of the limiting equation of a noisy consensus model in opinion dynamics. *J. Differ. Equations.*, **263**(1), 365–397. 1

Chen, W., Li, C. & Wang, G. (2010) On the stationary solutions of the 2D Doi–Onsager model. *Nonlinear Anal-Theor.*, **73**(8), 2410–2425. 1

Crandall, M. G. & Rabinowitz, P. H. (1971) Bifurcation from simple eigenvalues. *J. Funct. Anal.*, **8**(2), 321–340. 3.2, B

Davies, E. B. (2007) *Linear operators and their spectra*, volume 106. Cambridge University Press. B

De Gennes, P. & Prost, J. (1993) *The physics of liquid crystals*, volume 83. Oxford university press. 4.0.6

Diperna, R. & Lions, P.-L. (1988) Global weak solutions of kinetic equations. *Rend. Semin. Mat. Univ. Politec. Torino*, **46**(3), 259–288. 2

D'Orsogna, M. R., Chuang, Y., Bertozzi, A. L. & Chayes, L. S. (2006) Self-propelled particles with soft-core interactions: patterns, stability, and collapse. *Phys. Rev. Lett.*, **96**(10), 104302. 4.0.5

Dressler, K. (1987) Stationary solutions of the Vlasov-Fokker-Planck equation. *Math. Mathod. Appl. Sci.*, **9**(1), 169–176. 1, 2, 2, A

Goddard, B. D., Gooding, B., Pavliotis, G. A. & Short, H. (2020) Noisy bounded confidence models for opinion dynamics: the effect of boundary conditions on phase transitions. *arXiv preprint arXiv:2009.03131*. 1

Goddard, B. D., Nold, A. & Kalliadasis, S. (2016) Dynamical density functional theory with hydrodynamic interactions in confined geometries. *J. Chem. Phys.*, **145**(21), 214106. 4

Goddard, B. D., Nold, A. & Kalliadasis, S. (2017) 2DChebClass [Software]. http://dx.doi.org/10.7488/ds/1991. 4

Goddard, B. D., Nold, A., Savva, N., Pavliotis, G. A. & Kalliadasis, S. (2012a) General dynamical density functional theory for classical fluids. *Phys. Rev. Lett.*, **109**(12), 120603. 2, 4

Goddard, B. D., Pavliotis, G. A. & Kalliadasis, S. (2012b) The overdamped limit of dynamic density functional theory: Rigorous results. *Multiscale. Model. Sim.*, **10**(2), 633–663. 4

Gomer, R. (1990) Diffusion of adsorbates on metal surfaces. *Rep. Prog. Phys.*, **53**(7), 917. 1

Grauer, J., Löwen, H. & Liebchen, B. (2020) Strategic spatiotemporal vaccine distribution increases the survival rate in an infectious disease like Covid-19. *Sci. Rep.*, **10**(1), 1–10. 4.0.3

Hegselmann, R. & Krause, U. (2015) Opinion dynamics under the influence of radical groups, charismatic leaders, and other constant signals: A simple unifying model. *Netw. Heterog. Media*, **10**(3), 477. 1

Hérau, F. (2007) Short and long time behavior of the Fokker–Planck equation in a confining potential and applications. *J. Funct. Anal.*, **244**(1), 95–118. 2

Keller, E. F. & Segel, L. A. (1971) Model for chemotaxis. *J. Theor. Biol.*, **30**(2), 225–234. 1

Kuramoto, Y. (1981) Rhythms and turbulence in populations of chemical oscillators. *Physica A*, **106**(1-2), 128–143. 1, 4.0.7

Marconi, U. M. B. & Tarazona, P. (1999) Dynamic density functional theory of fluids. *J. Chem. Phys.*, **110**(16), 8032–8044. 2

Martzel, N. & Aslangul, C. (2001) Mean-field treatment of the many-body Fokker–Planck equation. *J. Phys. A-Math. Gen.*, **34**(50), 11225. 1, 4.0.3, 5

Messer, J. & Spohn, H. (1982) Statistical mechanics of the isothermal Lane-Emden equation. *J. Stat. Phys.*, **29**(3), 561–578. 2, 4.0.7

Mogilner, A., Edelstein-Keshet, L., Bent, L. & Spiros, A. (2003) Mutual interactions, potentials, and individual distance in a social aggregation. *J. Math. Biol*, **47**(4), 353–389. 4.0.5

Nold, A., Goddard, B. D., Yatsyshin, P., Savva, N. & Kalliadasis, S. (2017) Pseudospectral methods for density functional theory in bounded and unbounded domains. *J. Comput. Phys.*, **334**, 639–664. 4

Onsager, L. (1949) The effects of shape on the interaction of colloidal particles. *Ann. N. Y. Acad. Sci.*, **51**(4), 627–659. 4.0.6

Percus, J. K. (1976) Equilibrium state of a classical fluid of hard rods in an external field. *J. Stat. Phys.*, **15**(6), 505–511. 1

Rosenfeld, Y. (1989) Free-energy model for the inhomogeneous hard-sphere fluid mixture and density-functional theory of freezing. *Phys. Rev. Lett.*, **63**(9), 980. 1

Roth, R. (2010) Fundamental measure theory for hard-sphere mixtures: a review. *J. Phys.: Condens. Matter*, **22**(6), 063102. 1

Roth, R., Mecke, K. & Oettel, M. (2012) Communication: Fundamental measure theory for hard disks: Fluid and solid. . 1

Singh, Y. (1991) Density-functional theory of freezing and properties of the ordered phase. *Phys. Rep. Rev. Sec. Phys. Lett*, **207**(6), 351–444. 1

Tamura, Y. (1984) On asymptotic behaviors of the solution of a nonlinear diffusion equation. *J. Fac. Sci. U. Tokyo. 1A, Mathematics*, **31**(1), 195–221. 1

Te Vrugt, M., Bickmann, J. & Wittkowski, R. (2020) Effects of social distancing and isolation on epidemic spreading modeled via dynamical density functional theory. *Nat. Commun.*, **11**(1), 1–11. 1, 4.0.3

Victory Jr., H. D. & O'Dwyer, B. P. (1990) On classical solutions of Vlasov-Poisson Fokker-Planck systems. *Indiana U. Math. J.*, pages 105–156. 2

Wang, C., Li, Q., Weinan, E. & Chazelle, B. (2017) Noisy Hegselmann-Krause systems: phase transition and the 2r-conjecture. *J. Stat. Phys.*, **166**(5), 1209–1225. 1

Williams, E. D., Cunningham, S. L. & Weinberg, W. (1978) A determination of adatom–adatom interaction energies: Application to oxygen chemisorbed on the tungsten (110) surface. *J. Chem. Phys*, **68**(10), 4688–4693. 1

Zhdanov, V. P. & Kasemo, B. (1994) Kinetic phase transitions in simple reactions on solid surfaces. *Surf. Sci. Rep.*, **20**(3), 113–189. 1